Optics Letters

High-energy self-mode-locked Cr:forsterite laser near the soliton blowup threshold

Anatoly A. Ivanov,[1,2,3] Grigoriy N. Martynov,[1] Aleksandr A. Lanin,[1,3] Andrei B. Fedotov,[1,3] and Aleksei M. Zheltikov[1,3,4,*]

[1]Physics Department, International Laser Center, M.V. Lomonosov Moscow State University, Russia
[2]Center of Photochemistry, Crystallography and Photonics Federal Research Center, Russian Academy of Sciences, Moscow 119421, Russia
[3]Russian Quantum Center, Skolkovo, Moscow Region, Russia
[4]Department of Physics and Astronomy, Texas A&M University, College Station, Texas 77843, USA
*Corresponding author: zheltikov@physics.msu.ru

Received 2 December 2019; revised 24 January 2020; accepted 27 January 2020; posted 27 January 2020 (Doc. ID 384850); published 20 March 2020

At the level of peak powers needed for a Kerr-lens mode-locked operation of solid-state soliton short-pulse lasers, a periodic perturbation induced by spatially localized pulse amplification in a laser cavity can induce soliton instability with respect to resonant dispersive-wave radiation, eventually leading to soliton blowup and pulse splitting of the laser output. Here, we present an experimental study of a high-peak-power self-mode-locking Cr:forsterite laser, showing that, despite its complex, explosion-like buildup dynamics, this soliton blowup can be captured and quantitatively characterized via an accurate cavity-dispersion- and gain-resolved analysis of the laser output. We demonstrate that, with a suitable cavity design and finely tailored balance of gain, dispersion, and nonlinearity, such a laser can be operated in a subcritical mode, right beneath the soliton blowup threshold, providing an efficient source of sub-100-fs 15–20 MHz repetition-rate pulses with energies as high as 33 nJ.

https://doi.org/10.1364/OL.384850

Solid-state and fiber-optic soliton lasers (SLs) provide a powerful resource for ultrafast optical science and lightwave technologies [1,2]. Unlike their counterparts in standard passive optical fibers, where dispersion, nonlinearity, and gain are distributed continuously along the soliton propagation path, solitons in lasers are exposed to periodic perturbations as they are amplified in a gain medium within a laser cavity. In fiber-optic SLs, such periodic perturbations are known to induce a resonant coupling between solitons and dispersive waves (DWs), giving rise to Gordon–Kelly (GK) sidebands in the fiber-laser output spectrum [3,4], often accompanied by temporal instabilities and pulse splitting [5–8]. For solid-state SLs, on the other hand, such instabilities can usually be avoided [7] by keeping the nonlinear phase shift φ_{nl} per cavity round trip small enough to prevent resonant DW emission. However, as the SL operation regime is steered toward higher peak powers, in an attempt to meet the rapidly growing demand on high-repetition-rate, high-energy short-pulse sources, keeping the phase shift φ_{nl} small becomes difficult. GK sidebands inevitably show up in this regime [9], heralding soliton blowup and pulse splitting as an ultimate physical limit on the laser peak power.

The subcritical range of parameters near the threshold of this soliton blowup is thus of special interest, as it allows the highest peak powers to be achieved at the output of an SL (even higher output energies, albeit in much longer pulses, are attainable with positive-dispersion lasers [10–12]). In the experiments presented below, we study a near-threshold operation of a high-peak-power self-mode-locking Cr:forsterite (CrF) laser. Short-pulse CrF lasers [13–20] fill an important niche in ultrafast optical science and laser technologies [21], providing a powerful resource for nonlinear spectroscopy and microscopy [22–24], multimodal brain imaging [25], as well as high-energy supercontinuum generation [26,27]. With their output spectrum falling within one of the high-transmission windows of biological tissues, these laser sources provide larger penetration depths in nonlinear-optical bioimaging [25], making deeper regions of the brain and central nervous system accessible to the methods of opto- and thermogenetics [25,28]. The experiments presented in this Letter demonstrate that, with a suitable cavity design and accurately tailored balance of gain, dispersion, and nonlinearity, a self-mode-locking CrF laser can be operated in a subcritical mode, right beneath the soliton blowup threshold, providing an efficient source of sub-100-fs 15–20 MHz repetition-rate pulses with energies as high as 33 nJ, ideally suited for nonlinear microscopy, bioimaging, and neurophotonic applications [22–28].

In a typical short-pulse soliton fiber-laser setting, an energy boost that a soliton receives each time it is amplified in a gain medium does not match the soliton spectrally and temporally. Some fraction of this energy is therefore inevitably radiated in the form of a broadband DW packet as the amplified pulse reshapes into a soliton [3–5]. Each frequency component ω of this wave packet then acquires a dispersion-induced phase shift, φ_d, as it propagates through the laser cavity. The soliton pulse in the meantime acquires a phase shift of its own, φ_s. Back in the gain medium, the DW ω interferes with similar DWs emitted as a part of other pulse amplification events.

This interference is destructive unless the phase matching $\Delta\varphi_p = \varphi_s - \varphi_d = 2\pi m$, m being an integer, is achieved [6,7]. For a fiber-laser cavity with a period L_0, $\varphi_s = \beta_s L_0$ and $\varphi_d = \beta_d L_0$, where β_d and β_s are the propagation constants of the soliton and the DW at ω. Then, with the fiber dispersion included up to the third order, $\beta_d(\omega) \approx \sum_{k=0}^{3} \beta_k(\Delta\omega)^k/k!$, where $\beta_k = \partial^k\beta/\partial\omega^k$ at $\omega = \omega_0$ and $\Delta\omega = \omega - \omega_0$, the phase-matching condition $\Delta\varphi_p = 2\pi m$ translates [6, 8,] into the equation $3\beta_2 L_0(\Delta\omega_m^2 + \tau^{-2}) + \beta_3 L_0 \Delta\omega_m^3 \approx 12\pi m$ for GK sideband frequencies $\omega_m = \omega_0 + \Delta\omega_m$, with $\tau \approx \tau_p/1.76$, τ_p being the FWHM pulse width. Apart from the special case of sidebands with $m = 0$ [29], GK sideband soliton instabilities are rarely observed in the soliton output of solid-state lasers [7]. The $m = 0$ resonance, however, does not fully qualify as a GK sideband instability, as it in no way connects to the periodicity of soliton perturbation, but relates instead to a β_3-induced DW-emission soliton instability—an effect that has long been known and well understood for passive nonlinear fibers [30–32].

To gain insights into how GK sideband instabilities leading to a soliton blowup can show up in the output of a solid-state SL, we extend the soliton–DW coupling analysis to a typical solid-state laser setting. With dispersion included up to the third order, the phase-matching condition $\Delta\varphi_p = 0$ then leads to $3D_2(\Delta\omega_m^2 + \tau^{-2}) + D_3\Delta\omega_m^3 \approx 12\pi m$, where we introduced the net cavity group-delay dispersion (GDD) and third-order dispersion (TOD) $D_2 = 2\sum_j \beta_{2j} l_j$ and $D_3 = 2\sum_j \beta_{3j} l_j$, where β_{kj} is the β_k dispersion coefficient of the jth laser segment, l_j is the length of this segment, and the sum is over all the segments in the laser cavity. When expressed through the net cavity GDD and TOD, which, in the case of a fiber laser, are simply $D_2 = \beta_2 L_0$ and $D_3 = \beta_3 L_0$, the fiber-laser equation for $\Delta\omega_m$ is seen to become identical to its solid-state laser extension.

Even though the soliton peak power, P, does not even show up in the canonical form of the equation for GK sidebands, it is this equation that defines the upper bound on P for a stable single-pulse output of a SL. Indeed, the pulse width of the fundamental soliton τ, which explicitly enters this equation, relates to P via the soliton-area theorem. When extended to the solid-state SL setting, this theorem can be expressed as $P\tau^2 = |D_2|/\kappa$, where κ is found as a sum over all the segments in the laser cavity, $\kappa = 2\sum_j \gamma_j l_j$, $\gamma_j = (\omega/c)(n_{2j}/S_j)$, n_{2j} is the Kerr-effect nonlinear refractive index of the jth segment, and S_j is the mode area of the laser beam in the jth segment. Defined this way, parameter κ provides a measure for the total nonlinear phase accumulated by the laser pulse in all the laser components per unit peak power.

Using this modified soliton-area theorem to express τ^2 through P, we find from the equation for $\Delta\omega_m$ that growing P will push the GK sidebands toward the center of the soliton spectrum. As $\Delta\omega_1$ becomes much smaller than the soliton bandwidth, the soliton tends to lose its stability, giving way to pulse splitting and multiple-pulse lasing. Mathematically, this instability is described by frequency denominators in expressions for the amplitudes of GK sidebands, which display singularities, blowing up [3,6] GK sidebands at resonance frequencies ω_m. This soliton blowup sets an upper bound, P_{cr}, on the output peak power of a SL. With the TOD term in the equation for $\Delta\omega_m$ set equal to zero, we take $\Delta\omega_1 = 0$ as a meaningful criterion of soliton blowup to find $\kappa P_{cr} \approx \varphi_{nl} \approx 4\pi$ or $P_{cr} = 4\pi/\kappa$.

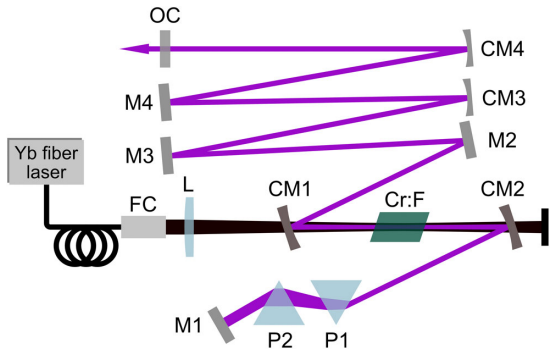

Fig. 1. Experimental setup: CrF, Cr: forsterite laser; M1–M8, mirrors; P1, P2, prisms; OC, output coupler; FC, fiber collimator.

In experiments, we work with a homebuilt CrF laser oscillator with a z-fold cavity design (Fig. 1). The overall single-pass length of the laser cavity L is varied from 5.5 to 10 m. A 15-mm-long $Cr^{4+}:Mg_2SiO_4$ crystal, placed between two concave mirrors with curvature radii of ≈ 10 cm, is driven by a 1030 nm output of a laser-diode-pumped Yb fiber laser with a variable power p. For a higher gain, the laser crystal is cooled down to a temperature of 278 to 290 K. A pair of SF57 prisms (P1 and P2 in Fig. 1) is used to tune the net cavity GDD D_2. Phase-resolved pulse characterization of the CrF laser output is performed by means of a frequency-resolved optical gating (FROG) based on second-harmonic generation (SHG). The spectra of laser pulses retrieved from SHG FROG traces are verified against the spectra measured with a standard OceanOptics spectrometer.

In agreement with standard models of soliton lasing [7,33], as well as with earlier studies of self-mode-locked CrF lasers [15–19], lower net cavity $|D_2|$ values favor the generation of shorter output pulses in our experimental setting. Specifically, with the cavity GDD set at $D_2 \approx -300$ fs^2 and a pump power of only $p \approx 6$ W, output pulses with $\tau_p \approx 50$ fs, $W \approx 11$ nJ, and $P \approx 0.22$ MW are delivered by our CrF laser at a pulse repetition rate $f \approx 15$ MHz.

As a general tendency, larger $|D_2|$ values allow the soliton operation of the CrF laser to be steered toward higher output peak powers and pulse energies. This result is fully consistent with the soliton-area theorem, as well as with the general design rules for SLs [7,8]. Shown by the blue curve in Fig. 2(a) is a typical spectrum of a high-P output of our CrF laser ($W \approx 21$ nJ, $f \approx 15$ MHz, $\tau_p \approx 55$ fs, $P \approx 0.38$ MW) adjusted for $D_2 \approx -400$ fs^2 with $p \approx 7.1$ W.

The output pulse energy can be further boosted by increasing the p pump power while carefully managing the cavity dispersion. In Fig. 2(a), we present the output spectra of the CrF laser measured with p kept constant at ≈ 8.8 W and with the net GDD D_2 varied from ≈ -1500 to 3200 fs^2 by adjusting the P1–P2 prism pair in the laser cavity. Changes in D_2 are seen to have a significant effect on the laser output. As larger $|D_2|$ is added, the output spectra become narrower, while the output pulse width increases, scaling, roughly, as $\sim |D_2|^{1/2}$. Deviations from this scaling in experiments are primarily due to TOD, which is inevitably added to the cavity as the P1–P2 prism pair is adjusted for a targeted $|D_2|$ value. The spectra of such pulses display well-resolved GK sidebands [Figs. 2(a)–2(d)], whose amplitudes rapidly increase as changes in D_2 and/or P push them toward the center of the soliton

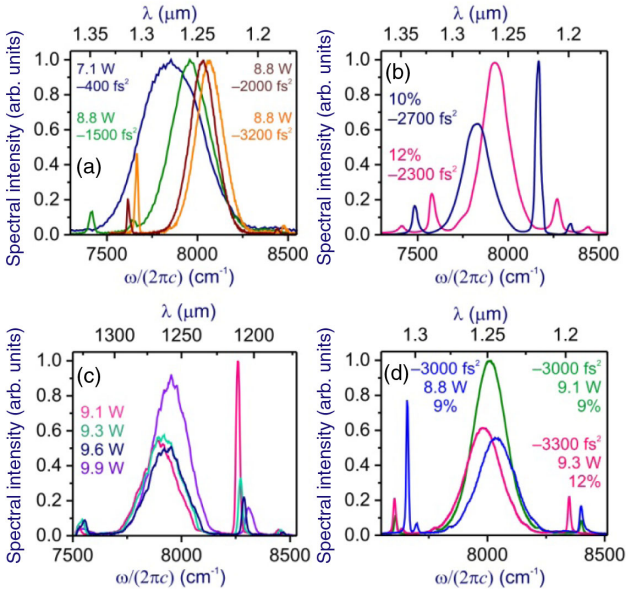

Fig. 2. Output spectra of the self-mode-locked CrF laser with (a) $p \approx 7.1$ W (blue curve) and 8.8 W (green, maroon, and orange curves), $D_2 \approx -400$ fs^2 (blue), -1500 fs^2 (green), -2000 fs^2 (maroon), and -3200 fs^2 (orange curve), $T \approx 8\%$; (b) $D_2 \approx -2700$ fs^2, $T \approx 10\%$ (blue) and $D_2 \approx -2300$ fs^2, $T \approx 12\%$ (red curve), $p \approx 8.7$ W; (c) $D_2 \approx -2400$ fs^2 and $p \approx 9.1$ W (blue), 9.3 W (green), 9.6 W (red), and 9.9 W (purple curve), $T \approx 15\%$; (d) $D_2 \approx -3000$ fs^2, $p \approx 8.8$ W, $T \approx 9\%$ (blue), $D_2 \approx -3000$ fs^2, $p \approx 9.1$ W, $T \approx 9\%$ (green), and $D_2 \approx -3300$ fs^2, $p \approx 9.3$ W, $T \approx 12\%$ (red).

spectrum at ω_0. In Fig. 2(a), this tendency is observed for laser output spectra measured with fixed p and T, but variable D_2, isolating the effect of GDD. The finding that GK sidebands with smaller $\Delta\omega_m$ are generated in cavities with larger $|D_2|$ [Fig. 2(a)] is fully consistent with the $\Delta\varphi_p = 0$ soliton–DW phase matching, which, in the case of small TOD, leads to $|\Delta\omega_m| \approx [(4\pi m - \kappa P)/D_2]^{1/2}$. The spectra shown in Fig. 2(c) are recorded with fixed D_2 and T, but variable p, illustrating effects of soliton peak power. Finally, Fig. 2(b) shows that solitons with close GK sideband frequencies, but drastically different sideband amplitudes can be generated through a fine tuning of D_2 and T at fixed p.

The sidebands in the spectra in Figs. 2(a)–2(d) are seen to be slightly asymmetric with respect to ω_0, indicating, in accordance with the equation for $\Delta\omega_m$, a weak, yet detectable, uncompensated TOD. As an instructive example, the laser output spectrum in Fig. 2(b) features two pairs of well-resolved GK sidebands with high- and low-frequency peaks at $\Delta\omega_{m+}$ and $\Delta\omega_{m-}$. The weakness of these sidebands indicates that the peak power of the soliton in this regime is well below the soliton blowup threshold, i.e., $\varphi_{nl} \approx \kappa P \ll 4\pi$. We can thus neglect the $|D_2|/\tau^2 \sim \kappa P$ term in the equation for $\Delta\omega_m$ and solve this equation iteratively, including the TOD term as a small correction to the GDD term. In the zeroth-order approximation, with $D_3 = 0$, we then find $\Delta\omega_{0m\pm} \approx \pm[(4\pi m - \kappa P)/D_2]^{1/2}$. Defining the sideband asymmetry parameter as $\delta_m = (\Delta\omega_{m+} - \Delta\omega_{m-})/\Delta\omega_{0m}$, with $\Delta\omega_{0m} = |\Delta\omega_{0m\pm}|$, we use the first-order solution for $\Delta\omega_{m\pm}$ to find $\delta_m \approx -[D_3/(6D_2)]\Delta\omega_{0m}$.

To be able to compare these results with experiments, we use the $\delta'_m = 2(\Delta\omega_{m+} - \Delta\omega_{m-})/(\Delta\omega_{m+} + \Delta\omega_{m-})$ ratio as a measure of sideband asymmetry in experimental spectra. For the laser output spectrum shown by the red line in Fig. 2(b), $D3/(6D_2) \approx -\delta'_1/\Delta\omega_{01} \approx -\delta'_2/\Delta\omega_{02} \approx 0.3$ fs and $D_3/(3D_2)]\Delta\omega_{0m} \approx 0.02$, confirming the smallness of TOD. In the regime where $P \ll P_{cr}$, the $D_2/\tau^2 \sim \kappa P$ term also becomes small. With both the TOD and the D_2/τ^2 terms dropped and with the experimental value $D_2 \approx -2500$ fs^2 used for the GDD term, the equation for $\Delta\omega_m$ gives $\Delta\omega_1/(2\pi c) \approx c^{-1}(\pi D_2)^{-1/2} \approx 380$ cm^{-1} and $\Delta\omega_2/\Delta\omega_1 \approx 1.4$. Both estimates are consistent with the experimental spectrum in Fig. 2(b), where $\Delta\omega_1/(2\pi c) \approx 350$ cm^{-1} and $\Delta\omega_2/\Delta\omega_1 \approx 1.4$. As P grows, the GK sidebands become highly sensitive to small variations in p. As one example, Fig. 2(c) presents laser output spectra measured for p growing from ≈ 9.1 to 9.9 W. An increase in p from $p_1 \approx 9.1$ W to $p_2 \approx 9.6$ W causes the pulse energy of the ≈ 95 fs laser output to grow from $W_1 \approx 29$ nJ to $W_2 \approx 32$ nJ, corresponding to an increase in the peak power from $P_1 \approx 0.31$ MW to $P_2 = P_1 + \Delta P \approx 0.34$ MW. The $m = 1$ GK sideband, which is observed at $\Delta\omega_1 \approx 420$ cm^{-1} for $P_1 \approx 0.31$ MW, is seen to shift in response to this change in P by $\delta\omega \approx 35$ cm^{-1} [Fig. 2(c)]. Remarkably, while the shift of the GK sideband changes by only $\approx 8\%$, its intensity increases by a factor of ≈ 5.

To understand this behavior of GK sidebands, we resort to the Gordon result for the rate of soliton energy transfer to a resonant DW within the mth-order GK sideband [3], $C_m \propto \mathrm{sech}^2(\pi\Delta\omega_m\tau/2)$. For the soliton with the peak power P_1 [blue line in Fig. 2(c)], $\Delta\omega' = \Delta\omega_1(P_1) \approx 420$ cm^{-1} and $\tau_1 = \tau(P_0) \approx 95$ fs, leading to $\Delta\omega'\tau_1 \approx 9 \gg 1$. In this limit, $\mathrm{sech}^2(\xi) \approx 4\exp(-2\xi)$ and $C_1 \propto \exp[-\pi(P_{cr}/P - 1)^{1/2}]$. Since $\Delta P/P_1 \approx 0.09 \ll 1$, we find $\delta\omega/\Delta\omega' \approx \Delta P/(2P_{cr})$ and $\theta(\Delta P) = C_1(P_2)/C_1(P_1) \approx \exp[\pi\Delta\omega'\tau_1\Delta P/(2P_1)]$. While $\delta\omega/\Delta\omega'$ scales linearly with ΔP, θ grows exponentially with $\Delta P/P_1$, in full agreement with experiments.

As a striking manifestation of soliton instability induced by resonant soliton–DW coupling above P_{cr}, with a pump power set at $p \approx 9.9$ W, i.e., only 3% above p_2, the pulse repetition rate doubles, indicating a double-pulse laser operation. SHG FROG traces measured in this regime of laser operation reveal the temporal structure of this double-pulse laser output [Fig. 3(a)]. Responding to this abrupt change in the peak power of individual laser pulses, the $m = 1$ GK sideband in the spectrum of the double-pulse laser output is shifted [purple line in Fig. 2(c)], in a similar jumpwise fashion, to $\Delta\omega_1 \approx 430$ cm^{-1}. Its intensity is seen to go down drastically, following the exponential scaling with ΔP, as predicted by the analysis of GK sidebands. A similar drastic change in the intensity of GK sidebands, indicative of soliton blowup, is seen in the CrF laser output spectra presented in Fig. 2(d) (cf. blue and green curves). This jumpwise change in sideband intensities is, once again, accompanied by f doubling, as another signature of soliton blowup, and is caused by an increase in p by only $\approx 3\%$.

In Fig. 3(b), we present a typical SHG FROG trace for a CrF laser operating near the soliton blowup threshold, with $P \approx 0.9P_{cr}$. The FROG trace calculated for the retrieved pulse shape, spectrum, and phase [Figs. 3(d) and 3(e)] agrees very well with the experimental FROG trace [cf. Figs. 3(b) and 3(c)], indicating an adequate accuracy of pulse characterization. The FWHM width of the laser pulse retrieved from FROG traces is

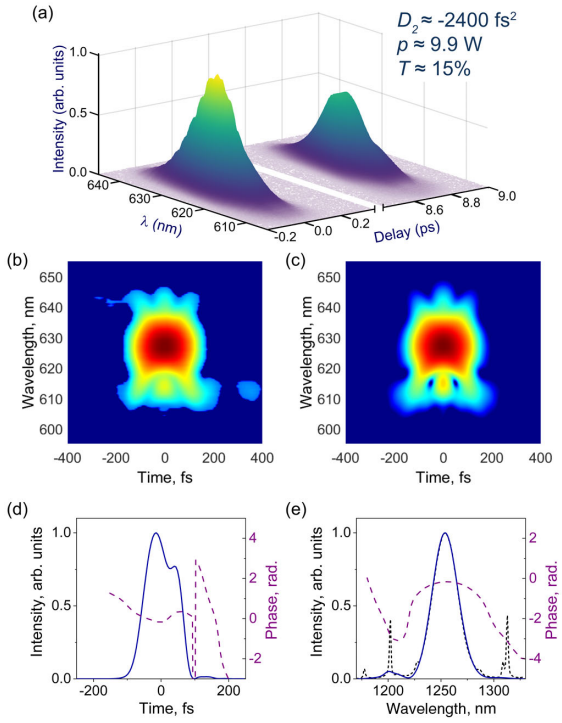

Fig. 3. (a) SHG FROG trace of a double-pulse laser output above P_{cr}. (b) Experimental and (c) retrieved SHG FROG traces of the CrF laser output. (d) The pulse shape (solid line) and temporal phase (dashed line) and (e) the spectrum (solid line) and spectral phase (dashed line) retrieved from SHG FROG measurements. Also shown is the spectrum of the pulse measured with a spectrometer (dotted line).

$\tau_p \approx 100$ fs. The pulse energy of the laser output in this regime is $W \approx 28$ nJ, corresponding to $P \approx 0.28$ MW. GK sidebands in the spectrum of this pulse indicate growing soliton instabilities. As a time-domain manifestation of these instabilities, the pulse shape of the laser output in Fig. 3(c) displays noticeable distortions. Both pulse-shape distortions and GK sidebands rapidly grow with the increase in p, eventually leading to a soliton blowup and pulse splitting at $P \approx P_{cr} \approx 0.33$ MW. As long as the TOD remains negligible, the soliton blowup threshold in experiments is accurately approximated as $P_{cr} \approx 4\pi/\kappa$.

To summarize, with a suitable cavity design and accurately tailored balance of gain, dispersion, and nonlinearity, self-mode-locking CrF lasers can be operated in a subcritical mode right beneath the soliton blowup threshold. In this regime, CrF lasers can deliver sub-100-fs 15–20 MHz repetition-rate pulses with pulse energies as high as 33 nJ and peak powers in excess of 0.3 MW at the level of pump powers of 8–10 W.

Funding. Russian Foundation for Basic Research (18-29-20031, 19-02-00473, 18-02-40025, 18-02-01091, 18-32-20191); Russian Science Foundation; Welch Foundation (A-1801-20180324).

Acknowledgment. We thank A. A. Voronin for the valuable help.

Disclosures. The authors declare no conflicts of interest.

REFERENCES

1. L. F. Mollenauer and R. H. Stolen, Opt. Lett. **9**, 13 (1984).
2. H. A. Haus, IEEE J. Sel. Top. Quantum Electron. **6**, 1173 (2000).
3. J. P. Gordon, J. Opt. Soc. Am. B **9**, 91 (1992).
4. S. M. Kelly, Electron. Lett. **28**, 806 (1992).
5. D. U. Noske, N. Pandit, and J. R. Taylor, Opt. Lett. **17**, 1515 (1992).
6. L. F. Mollenauer, J. P. Gordon, and M. N. Islam, IEEE J. Quantum Electron. **22**, 157 (1986).
7. L. E. Nelson, D. J. Jones, K. Tamura, H. A. Haus, and E. P. Ippen, Appl. Phys. B **65**, 277 (1997).
8. M. L. Dennis and M. L. I. N. Duling, III, IEEE J. Quantum Electron. **30**, 1469 (1994).
9. A. A. Ivanov, A. A. Voronin, A. A. Lanin, D. A. Sidorov-Biryukov, A. B. Fedotov, and A. M. Zheltikov, Opt. Lett. **39**, 205 (2014).
10. H. Cankaya, S. Akturk, and A. Sennaroglu, Opt. Lett. **36**, 1572 (2011).
11. M. Siegel, N. Pfullmann, G. Palmer, S. Rausch, T. Binhammer, M. Kovacev, and U. Morgner, Opt. Lett. **34**, 740 (2009).
12. V. L. Kalashnikov and A. Apolonski, Phys. Rev. A **79**, 043829 (2009).
13. A. Seas, V. Petričević, and R. R. Alfano, Opt. Lett. **18**, 891 (1993).
14. V. Yanovsky, Y. Pang, F. Wise, and B. I. Minkov, Opt. Lett. **18**, 1541 (1993).
15. B. Chassagne, G. Jonusauskas, J. Oberlé, and C. Rullière, Opt. Commun. **150**, 355 (1998).
16. Z. Zhang, K. Torizuka, T. Itatani, K. Kobayashi, T. Sugaya, T. Nakagawa, and H. Takahashi, Opt. Lett. **23**, 1465 (1998).
17. A. A. Ivanov, M. V. Alfimov, and A. M. Zheltikov, Laser Phys. **10**, 796 (2000).
18. C. Chudoba, J. G. Fujimoto, E. P. Ippen, H. A. Haus, U. Morgner, F. X. Kärtner, V. Scheuer, G. Angelow, and T. Tschudi, Opt. Lett. **26**, 292 (2001).
19. A. B. Fedotov, A. A. Voronin, I. V. Fedotov, A. A. Ivanov, and A. M. Zheltikov, Opt. Lett. **34**, 662 (2009).
20. S.-H. Chia, T.-M. Liu, A. A. Ivanov, A. B. Fedotov, A. M. Zheltikov, M.-R. Tsai, M.-C. Chan, C.-H. Yu, and C.-K. Sun, Opt. Express **18**, 24085 (2010).
21. A. A. Ivanov, M. V. Alfimov, and A. M. Zheltikov, Phys. Usp. **47**, 687 (2004).
22. S.-W. Chu, I.-H. Chen, T.-M. Liu, P. Chen, C.-K. Sun, and B.-L. Lin, Opt. Lett. **26**, 1909 (2001).
23. S. O. Konorov, D. A. Akimov, E. E. Serebryannikov, A. A. Ivanov, M. V. Alfimov, and A. M. Zheltikov, Phys. Rev. E **70**, 057601 (2004).
24. L. V. Doronina-Amitonova, A. A. Lanin, O. Ivashkina, M. Zots, A. Fedotov, K. V. Anokhin, and A. M. Zheltikov, Appl. Phys. Lett. **99**, 231109 (2011).
25. M. S. Pochechuev, A. A. Lanin, I. V. Kelmanson, D. S. Bilan, D. A. Kotova, A. S. Chebotarev, V. Tarabykin, A. B. Fedotov, V. V. Belousov, and A. M. Zheltikov, Opt. Lett. **44**, 3166 (2019).
26. A. B. Fedotov, A. A. Voronin, I. V. Fedotov, A. A. Ivanov, and A. M. Zheltikov, Opt. Lett. **34**, 851 (2009).
27. L. Haizer, I. Bugar, E. Serebryannikov, D. Lorenc, F. Uherek, E. Goulielmakis, and A. Zheltikov, Opt. Lett. **39**, 5562 (2014).
28. A. A. Lanin, M. S. Pochechuev, A. S. Chebotarev, I. V. Kelmanson, V. V. Belousov, and A. M. Zheltikov, J. Biophoton. **12**, e201800432 (2019).
29. P. F. Curley, Ch. Spielmann, T. Brabec, F. Krausz, E. Wintner, and A. J. Schmidt, Opt. Lett. **18**, 54 (1993).
30. N. Akhmediev and M. Karlsson, Phys. Rev. A **51**, 2602 (1995).
31. J. M. Dudley, G. Genty, and S. Coen, Rev. Mod. Phys. **78**, 1135 (2006).
32. A. M. Zheltikov, Phys. Usp. **49**, 605 (2006).
33. F. Krausz, M. E. Fermann, T. Brabec, P. F. Curley, M. Hofer, M. H. Ober, C. Spielmann, E. Wintner, and A. J. Schmidt, IEEE J. Quantum Electron. **28**, 2097 (1992).